

# Orbital parameters and activity of ZZ Tau – a low mass young binary with circumbinary disc

A. Belinski,<sup>1</sup> M. Burlak,<sup>1</sup> A. Dodin,<sup>1</sup> N. Emelyanov,<sup>1</sup> N. Ikonnikova,<sup>1</sup> S. Lamzin,<sup>1\*</sup>  
B. Safonov,<sup>1</sup> and A. Tatarnikov<sup>1</sup>

<sup>1</sup> *Sternberg Astronomical Institute, Moscow M.V. Lomonosov State University, Universitetskij pr., 13, Moscow, 119992, Russia*

Accepted

. Received

; in original form

## ABSTRACT

We present the results of our new observations of the young binary ZZ Tau with a circumbinary disc. The system was found to consist of two coeval (age < 2 Myr) classical T Tauri stars with the total mass  $0.86 \pm 0.09 M_{\odot}$ , orbital period  $46.8 \pm 0.8$  yr, semimajor axis  $88.2 \pm 2.1$  mas, eccentricity  $0.58 \pm 0.02$  and the orbital inclination  $123^{\circ}8 \pm 1^{\circ}0$ . The accretion rate of ZZ Tau A and ZZ Tau B are approximately  $7 \times 10^{-10}$  and  $2 \times 10^{-10} M_{\odot} \text{ yr}^{-1}$ , respectively. No correlation was found between the long-term photometric variability of ZZ Tau and orbital position of its components. The periodic light variations with  $P = 4.171 \pm 0.002$  days was observed in the *BVRI* bands presumably connected with an accretion (hot) spot on the surface of the primary (ZZ Tau A). At the same time no periodicity was observed in the *U* band nor in the emission line profile variations probably due to the significant contribution of ZZ Tau B's emission, which dominates shortward of  $\lambda \approx 0.4 \mu\text{m}$ . We argue that the extinction in the direction to the primary is noticeably larger than that to the secondary. It appeared that the rotation axis of the primary is inclined to the line of sight by  $\approx 31^{\circ} \pm 4^{\circ}$ . We concluded also that ZZ Tau is the source of an CO molecular outflow, however, ZZ Tau IRS rather than ZZ Tau is the source of the Herbig-Haro object HH393.

**Key words:** binaries: general – stars: variables: T Tauri, Herbig Ae/Be – stars: individual: ZZ Tau, ZZ Tau IRS – accretion, accretion discs – stars: winds, outflows.

## 1 INTRODUCTION

In the last two decades, some young binary stars were discovered whose orbital plane is noticeably inclined to the circumbinary (CB) disc (Smallwood et al. 2021). At first glance, it seems that this fact contradicts the idea that the binary and its CB disc were formed from the same protostellar cloud. But the star formation in turbulent molecular cloud may lead to chaotic accretion, as a result of which the misalignment between the disc and orbital plane of a binary may occur (Monin et al. 2007; Bate et al. 2010; Wurster et al. 2019). Such systems can also originate from dynamical encounters during star cluster formation (Bate 2018).

Martin & Lubow (2017) and Zanazzi & Lai (2018) have shown that if a binary system has a noticeable eccentricity, then the initially small  $\Theta$  angle between the orbital plane and the CB disc either gradually decreases to zero or in-

creases to  $90^{\circ}$  in a time-scale less than the disc lifetime. It means that it is important to study young binaries with different values of  $\Theta$  to better understand the process of star and planet formation.

Here we consider a low mass young binary ZZ Tau with a CB disc. The aim of the paper is to specify orbital parameters of the binary and to discuss possible relation of the binary components activity to the presence of a CB disc.

ZZ Tau is located within the dark cloud filament Barnard 18 (Myers 1982). Its irregular variability in the range  $12^{\text{m}}9 - 15^{\text{m}}2$  pg was discovered by Reinmuth (1930). Herbig & Kameswara Rao (1972) included the star into the ‘Second Catalog of Emission Line Stars of the Orion Population’ and noted that ‘only Ca II H,K lines have been observed in emission.’ Later Herbig & Bell (1988) detected the emission lines of He I and H $\alpha$  (with an equivalent width of  $EW_{\text{H}\alpha} = 15 \text{ \AA}$ ), so ZZ Tau was classified as a T Tauri (TTS) M3 type star in their Catalog (HBC 46).

The *Gaia* parallax for ZZ Tau (*Gaia* EDR3 id 147869784062378624) is  $7.46 \pm 0.14$  mas, which corresponds

\* E-mail: lamzin@sai.msu.ru

to a distance of  $134 \pm 3$  pc (Gaia Collaboration et al. 2016, 2020). But the respective astrometric solution is not reliable with a renormalized unit weight error of 6.64, so we will further use the distance  $d = 140$  pc as in the paper of Schaefer et al. (2014).

The 1991 lunar occultation observation of Simon et al. (1995) revealed that ZZ Tau is a binary system with a projected separation of 29 mas. Schaefer et al. (2014) found from the analysis of the previous (Schaefer et al. 2003, 2006) and new observations the following orbital parameters of the system: period  $P \approx 46$  yr, semimajor axis  $a \approx 12$  au, eccentricity  $e \approx 0.57$ . It was also concluded that the system consists of M2.5+M3.5 stars with a total mass of  $M_A + M_B \approx 0.8 M_\odot$  and an age of  $< 3$  Myr in agreement with later estimation of Zhang et al. (2018).

The spectral energy distribution (SED) of ZZ Tau A+B demonstrates an excess emission longward of  $\lambda \approx 4 \mu\text{m}^1$  and prominent silicate features between 8 and 21  $\mu\text{m}$  (Sargent et al. 2009). Analyzing these features Espaillat et al. (2012) concluded that at least one component of the binary has an optically thick accretion disc – see also Fig. 7 and 8 in Furlan et al. (2011). It can be assumed that the accretion of disc’s matter is the reason for the observed short wavelength excess emission in the optical (Herczeg & Hillenbrand 2014) and UV (Gómez de Castro et al. 2015) spectra of ZZ Tau A+B. The accretion rate estimations  $\dot{M}_{\text{acc}}$  based on the analysis of similar (spatially unresolved) spectra, vary between  $2 \times 10^{-10}$  (Cieza et al. 2012) and  $1.3 \times 10^{-9} M_\odot \text{yr}^{-1}$  (Valenti et al. 1993).

The minimal distance between the components of the binary is  $a(1 - e) < 6$  au, so one can expect that the outer radii of their circumstellar discs are  $\lesssim 3$  au due to dynamical interaction (Artymowicz & Lubow 1994). According to Espaillat et al. (2012) it means that the mass of these discs  $M_{\text{disc}}$  is  $\lesssim 2 \times 10^{-5} M_\odot$  in agreement with the observed upper limit of  $4 \times 10^{-4} M_\odot$  (Andrews & Williams 2005; Andrews et al. 2013). Probably it explains why only weak continuum flux in 70 and 100  $\mu\text{m}$  bands and no line emission (e.g. [O I] 63  $\mu\text{m}$ ) was observed by Howard et al. (2013).

As far as  $M_{\text{disc}}/\dot{M}_{\text{acc}}$  time-scale is an order of magnitude less than the age of the binary, the inner circumstellar discs should be replenished in some way. But the mass of the circumbinary disc of ZZ Tau A+B found by Akeson et al. (2019) from ALMA observations appears too small ( $\log M_{\text{disc}}/M_\odot = -4.24 \pm 0.11$ ) to solve the problem. Then the question arises: whether the blue excess emission of ZZ Tau does refer to the accretion rather than to the chromospheric activity.

Neither forbidden lines nor other indications to outflow activity were found in the optical (Valenti et al. 1993; Kenyon et al. 1998; Herczeg & Hillenbrand 2014) and near IR (Folha & Emerson 2001) spectra of ZZ Tau A+B. At the same time Heyer et al. (1987) found monopolar redshifted  $^{12}\text{CO}$ -outflow presumably from ZZ Tau, while

<sup>1</sup> Large veiling  $r = 0.7_{-0.1}^{+0.3}$  of the ZZ Tau’s spectrum at  $\lambda = 4.7 \mu\text{m}$  found by Doppmann et al. (2017) may be due to the fact that the authors erroneously used in their analysis  $T_{\text{eff}}$  and  $\log g$  of ZZ Tau IRS – another young star located  $\approx 35''$  to the south from ZZ Tau (Gomez et al. 1997).

**Table 1.** Optical photometry of ZZ Tau A+B

rJD	<i>U</i>	$\sigma_U$	<i>B</i>	$\sigma_B$	<i>V</i>	$\sigma_V$	<i>R</i>	$\sigma_R$	<i>I</i>	$\sigma_I$
8382.51			15.78	0.10	14.37	0.02	13.10	0.07	11.19	0.10
9104.508	15.88	0.05								
9187.550	15.35	0.05	15.91	0.07	14.37	0.03	12.93	0.06	11.18	0.10

The Table is available in its entirety in a machine-readable form in the online journal. A portion is shown here for guidance regarding its form and content.

Narayanan et al. (2012) noted that the morphology of the outflow admits the possibility that ZZ Tau IRS is the source of the outflow. Besides, Gomez et al. (1997) detected an [S II] emission knot, presumably a Herbig-Haro object (HH 393), and argued that ZZ Tau IRS is the driving source for this outflow, but Bally et al. (2012) suppose that its source is ZZ Tau.

Schaefer et al. (2014) wrote: ‘we suspect that the orbital parameters’ of the binary ‘will be revised substantially in the future.’ As we have seen, the physical parameters of ZZ Tau’s components as well as the nature of their activity also need to be clarified.

The rest of the paper is organized in the following way. Initially we describe our observations (Section 2) and then present and discuss the results in Section 3. Section 4 is devoted to the problems related to circumstellar environment of the binary. Finally, we summarize the conclusions.

## 2 OBSERVATIONS

The unresolved photometry of ZZ Tau A+B was carried out with the 0.6-m telescope of the Caucasian Mountain Observatory (CMO) of Sternberg Astronomical Institute of Lomonosov Moscow State University (SAI MSU) equipped with a CCD camera and a set of standard Bessel-Cousins *UBVR<sub>c</sub>* filters (Berdnikov et al. 2020). Two additional observations in the same bands were performed with the 2.5-m telescope of the CMO equipped with a mosaic CCD camera and a set of similar *UBVRI* filters. One can find a more detailed description of the equipment, observational routine and data reduction procedures in Dodin et al. (2019). A single set of comparison stars was used through all the observations, the *BVRI* magnitudes for them were adopted from AAVSO<sup>2</sup>. The stars are: 000-BLB-648, 000-BLR-132, 000-BLR-134, 000-BLB-650, 000-BLR-079, 000-BLR-133. For the *U* band, we adopted the comparison star XEST 13-OM-054 from Audard et al. (2007).

Results of our photometry are presented in Table 1<sup>3</sup>.

The unresolved near infrared (NIR) observations of ZZ Tau were carried out between 2015 December and 2021 November in the *JHK* bands of the MKO photometric system at the 2.5-m telescope of CMO SAI MSU equipped with the infrared camera-spectrograph ASTRONIRCAM (Nadjip et al. 2017). The details of observations and data

<sup>2</sup> <https://www.aavso.org>

<sup>3</sup> rJD abbreviation in the first column of the Table means a reduced Julian Date rJD = JD – 2 450 000 and will be used below as well.

**Table 2.** NIR photometry of ZZ Tau A+B

rJD	$J$	$\sigma_J$	$H$	$\sigma_H$	$K$	$\sigma_K$
9079.528	9.42	0.01	8.74	0.03	8.42	0.03
9084.487	9.41	0.01	8.73	0.03	8.39	0.02
9091.572	9.45	0.03	8.78	0.05	8.44	0.01
9094.494	9.43	0.01	8.73	0.02	8.46	0.02
9551.258	9.54	0.07	8.76	0.02	8.45	0.03

**Table 3.** Optical polarimetry of ZZ Tau A+B in  $I$  band.

rJD	$p$	$\sigma_p$	$\theta$	$\sigma_\theta$
	%	%	°	°
7818.25	0.27	0.03	118.6	3.4
7820.22	0.34	0.03	118.2	2.6
9514.52	0.21	0.07	116.9	8.9
9517.43	0.28	0.04	122.9	3.8

Col. 1: Date of observation; Col. 2–3: the polarization degree and its error; Col. 4–5: the polarization angle and its error;

reduction are described in [Dodin et al. \(2019\)](#), the results are presented in Table 2.

We also carried out polarimetric observations of ZZ Tau A+B in the  $I_c$  band with the SPeckle Polarimeter (SPP) of the 2.5-m telescope of SAI MSU ([Safonov et al. 2017](#)). The details of observations and data reduction are described in [Dodin et al. \(2019\)](#), the results are presented in Table 3.

SPP was also used for speckle interferometric observations of ZZ Tau. Observations were carried out on 2019, December, 17 and 2021, October, 27 in the passband centered at  $0.9 \mu\text{m}$ , which is close to (but does not coincide with) the  $I_c$  band. The difference of the binary components magnitudes at these moments were  $0.71 \pm 0.10$  and  $0.65 \pm 0.10$ . Respective values of angular separation  $\rho$  and position angle  $PA$  are presented in two last rows of Table 5.

For our study we have additionally used high and medium resolution optical spectra of ZZ Tau taken from the archives of the following telescopes: Keck (HIRES spectrograph, spectral resolution  $R = \lambda/\Delta\lambda \approx 48\,000$ , PI D. Scott),<sup>4</sup> Canada-France-Hawaii (ESPaDOnS,  $R \approx 65\,000$ , PI L. Cieza),<sup>5</sup> and Very Large Telescope:<sup>6</sup> spectrographs UVES ( $R \approx 42\,000$ , PI E. Moraux) as well as MUSE ( $R \approx 2500$ , PI S. Haefert). The spectra obtained with HIRES, ESPaDOnS and UVES spectrographs are combined spectra of both components of ZZ Tau, whereas MUSE resolves the spectra of each component of the binary. Some additional information about these spectra and their abbreviated names that will be used below are presented in Table 4.

All the spectra are marked as a ‘scientific grade’ in the archives, so we did not process them additionally. The spectra of ZZ Tau observed with the HIRES and ESPaDOnS spectrographs are normalised to the continuum level, whereas the spectra observed with the UVES and

**Table 4.** Spectra of ZZ Tau analysed in this paper

Object	Date, UT	Name	Band, nm
ZZ Tau A+B	2008-Dec-04, 14:02	HIRES	445-890
	2009-Sep-30, 01:26	ESP-1	370-1048
	2010-Jul-30, 03:22	ESP-2	370-1048
	2010-Dec-17, 01:26	ESP-3	370-1048
	2018-Nov-27, 07:00	UVES-1	473-684
	2018-Dec-07, 06:19	UVES-2	473-684
	2018-Dec-24, 01:58	UVES-3	473-684
ZZ Tau A, B	2020-Jan-14, 02:07	MUSE	475-935

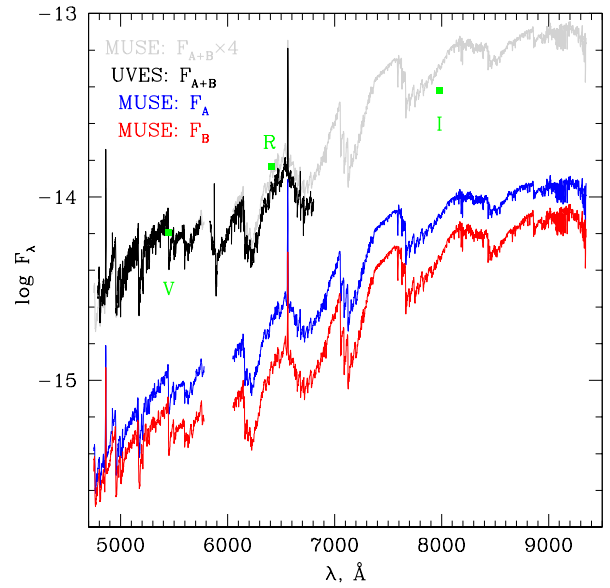


**Figure 1.** Observed MUSE spectra of ZZ Tau A (blue) and ZZ Tau B (red). The sum of component’s spectra increased by 4 times (grey) is shown to reconcile with our photometric measurements in the  $V$ ,  $R$  and  $I$  bands (green squares) as well as with the UVES-1 spectrum of ZZ Tau A+B degraded to spectral resolution  $R=2500$  (black). The flux is in units  $\text{erg s}^{-1} \text{cm}^{-2} \text{\AA}^{-1}$ . See text for details.

MUSE spectrographs are flux calibrated. However, the sum of *absolute* fluxes of ZZ Tau A and B components in the MUSE spectrum appeared  $\approx 4$  times less than the fluxes corresponding to our  $VRI$  photometric data – see Fig. 1. In contrast, all the three UVES spectra, which by the way coincide with each other (but see Sect. 3.4), are in agreement with the results of our  $V$  and  $R$  photometry. As can be seen from the figure, the UVES spectra also coincide with the 4 times increased combined MUSE spectrum up to  $\approx 0.62 \mu\text{m}$ , i.e. almost in the entire  $V$  band.

We did not find the source of wrong flux calibration of the MUSE spectra, and did not use information about the absolute fluxes of ZZ Tau from these spectra in our study. At the same time we have no reason to doubt that the flux ratio of ZZ Tau’s components in the MUSE spectrum shortward of  $\sim 0.6 \mu\text{m}$  is correct.

<sup>4</sup> <https://koa.ipac.caltech.edu/cgi-bin/KOA/nph-KOALogin>

<sup>5</sup> <http://www.cadc-ccda.hia-ihp.nrc-cnrc.gc.ca/en/>

<sup>6</sup> <http://archive.eso.org/scienceportal/home>

**Table 5.** Astrometric observations of ZZ Tau

Date yr	$\rho$ mas	$\sigma_\rho$ mas	PA °	$\sigma_{PA}$ °	Ref.
1995.081	36.0	7.6	187.0	11	1
1996.124	36.0	7.6	177.0	10	1
1997.704	50.6	5.4	129.2	6.0	1
1998.214	55.0	5.4	125.0	6.0	1
1999.621	57.9	1.3	112.9	1.8	1
2000.564	59.5	1.2	106.2	1.8	1
2000.690	58.2	1.2	105.7	1.8	1
2001.646	62.5	1.1	98.9	1.8	1
2002.748	60.6	1.3	91.1	1.7	1
2002.929	61.2	1.5	88.8	1.5	1
2003.723	62.8	1.5	87.6	1.4	2
2004.982	61.32	1.35	74.02	1.26	3
2005.849	61.7	1.5	67.2	1.4	2
2006.963	66.31	1.21	61.39	1.05	3
2008.045	66.31	0.49	54.09	0.42	3
2008.962	67.75	0.55	48.80	0.47	3
2011.065	73.02	1.05	38.39	0.82	3
2011.780	74.10	0.41	33.89	0.32	3
2013.074	76.77	1.56	23.74	1.16	3
2014.068	79.52	0.63	23.37	0.46	3
2019.961	93.5	2	0.5	1.0	4
2021.819	99.0	1	358.1	0.8	4

1 – Schaefer et al. (2003), 2 – Schaefer et al. (2006),  
3 – Schaefer et al. (2014), 4 – this work. Additional  
information from 1991.592 lunar occultation:  $\rho = 29$  mas to  
PA = 244° (Simon et al. 1995).

### 3 RESULTS AND DISCUSSION

#### 3.1 The Orbit

To calculate the orbit of ZZ Tau we used the same observational data as Schaefer et al. (2014) – see Table 5 – including the constraints implied by the 1991.6 lunar occultation observation of Simon et al. (1995) and added the results of our measurements. The orbit was determined by the differential refinement of orbital parameters using the least squares method (see Emelyanov (2020) for details). Weights were assigned to the observations according to the errors given by the observers. The observed minus calculated positions were found for each observation. For these deviations the RMS of the post fit to the complete data set are equal to 3.1 mas for an unweighted observation and to 0.98 mas for a weighted one.

As can be seen from comparing the first and the second rows of Table 6, our values of orbital period  $P$ , time of periastron passage  $T_0$ , eccentricity  $e$ , (angular) semimajor axis  $a$ , orbital inclination  $i$ , position angle of ascending node  $\Omega$ , argument of periastron  $\omega$  and total mass of the components  $M_A + M_B$  are very close to the respective values found by Schaefer et al. (2014) but more accurate. As far as ZZ Tau is a visual binary,  $\omega$  is given for the secondary. With the adopted distance to the binary 140 pc its semimajor axis in linear scale is  $a \approx 12.3$  au.

If using only astrometric data, it is not possible to determine which node of the orbit is ascending and which is descending. In other words the projection of the orbit to the celestial sphere will be the same as in the case of a ‘mirror’ orbit, when the position angle of the ascending node  $\Omega$  and the argument of periastron  $\omega$  presented in the Table 6 are

simultaneously replaced by  $\Omega + 180^\circ$  and  $\omega - 180^\circ$ , respectively – see the third row in the table. This ambiguity can be eliminated by the fact that the observed radial velocity of the companion relative to the primary  $\Delta V_r = V_r^B - V_r^A$  in both cases takes the same absolute value in each point of the orbit, but with opposite signs.<sup>7</sup>

Indeed, if  $v$  is a true anomaly, i.e. the angle in the orbital plane between the directions to the periastron and the companion viewed from the primary, then it can be shown that (Emelyanov 2020):

$$\Delta V_r = V_0 [\cos(v + \omega) + e \cos \omega], \quad (1)$$

where, according to Table 6,

$$V_0 = \sqrt{\frac{G(M_A + M_B)}{a(1 - e^2)}} \times \sin i \approx 7.94 \text{ km s}^{-1}. \quad (2)$$

Thus,  $\Delta V_r$  varies between approximately  $-6.0$  and  $+9.9 \text{ km s}^{-1}$ , if  $\omega = 294.9^\circ$ , or between  $-9.9$  and  $+6.0 \text{ km s}^{-1}$  in the case of the mirror orbit ( $\omega = 114.9^\circ$ ).

Radial velocity measurements based on spatially resolved NIR spectra of ZZ Tau’s components (obtained with NIRSPA0 at the Keck Observatory) were kindly presented to us by L.Prato on our request.<sup>8</sup> The results of these measurements (with errors of  $< 1 \text{ km s}^{-1}$ ) are presented in Table 7 along with the theoretical  $\Delta V_r$  values calculated from Eq.(1) for the moments of respective observations, so that a ‘plus’ sign of these values corresponds to the values of  $\omega$  and  $\Omega$  from the second row of Table 6, whereas a ‘minus’ sign corresponds to the ‘mirror’ orbit. As far as the observed  $\Delta V_r$  values are negative the mirror orbit looks preferable, but see Sect. 3.4.

The comparison of observational data with the mirror orbit is shown in Fig. 2, so that the part of the orbit that is closer to the Earth than ZZ Tau A ( $z < 0$ ) is shown with a solid line, so the  $N_1$  point corresponds to the ascending node. The weighted standard deviation  $\sigma$  of theoretical orbit from observational data is  $\approx 1.0$  mas. We believe that our orbit reproduces the observations fairly well, so the discrepancy between the theoretical and observed  $\Delta V_r$  values in Table 7 requires an explanation. We will discuss a possible reason for this disagreement in Sect. 3.4.

It follows from our solution that the minimal and maximum distances between the binary components are  $r_{\min} = a(1 - e) \approx 5.2$  and  $r_{\max} = a(1 + e) \approx 19.5$  au, respectively, and the mass of the system is  $M_A + M_B = 0.86 \pm 0.09 M_\odot$ .

#### 3.2 Photometry

The historical light curve of ZZ Tau A+B, shown in Fig. 3, was constructed from our  $B$  and  $V$  data (see Table 1) and the data adopted from the literature (Reinmuth 1930; Malyshev 1972; Kirillova & Pavlovskaya 1963; Rydgren & Vrba 1983; Nurmanova 1983; Schaefer et al. 2003). The cross in the upper panel of the figure corresponds to the information from Himpel (1944) that the 5 visual brightness estimations made

<sup>7</sup> We used a Cartesian coordinate system with the origin in the primary, the  $XY$  plane coinciding with the celestial sphere and the  $X$ ,  $Y$  and  $Z$  axes directed to the north pole  $N$ , east  $E$  and from the Earth to the star, respectively.

<sup>8</sup> See also <http://jumar.lowell.edu/BinaryStars/>

**Table 6.** Orbital parameters of ZZ Tau

Source	$P$ yr	$T_0$ yr	$e$	$a$ mas	$i$ °	$\Omega$ °	$\omega$ °	$M_A + M_B$ $M_\odot$
Schaefer et al. (2014)	$46.2 \pm 2.8$	$1995.01 \pm 0.28$	$0.57 \pm 0.03$	$86.4 \pm 4.5$	$124.6 \pm 2.0$	$137.0 \pm 2.3$	$294.9 \pm 2.3$	$0.83 \pm 0.16$
This work	$46.8 \pm 0.8$	$1995.07 \pm 0.13$	$0.58 \pm 0.02$	$88.2 \pm 2.1$	$123.8 \pm 1.0$	$136.7 \pm 1.3$	$294.9 \pm 0.9$	$0.86 \pm 0.09$
Mirror orbit	$46.8 \pm 0.8$	$1995.07 \pm 0.13$	$0.58 \pm 0.02$	$88.2 \pm 2.1$	$123.8 \pm 1.0$	$316.7 \pm 1.3$	$114.9 \pm 0.9$	$0.86 \pm 0.09$

**Table 7.** Radial velocity ( $\text{km s}^{-1}$ ) of ZZ Tau’s components

Component	2009, Dec 06	2010, Dec 10
ZZ Tau A	+16.20	+15.77
ZZ Tau B	+15.35	+13.64
$\Delta V_r$ , obs	-0.85	-2.13
$\Delta V_r$ , theor	$\pm 1.69$	$\pm 1.27$

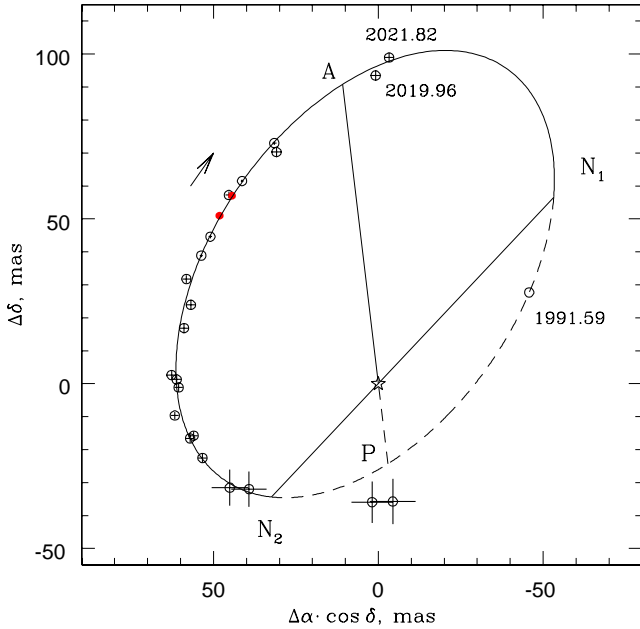


**Figure 2.** Variations of relative position of components in ZZ Tau. Open circles correspond to observation used to calculate the orbit.  $A$ ,  $P$  letters mark the position of apoastron and periastron, respectively, and  $N_1 - N_2$  is the line of nodes, so that  $N_1$  is the ascending node. The origin of the coordinate system is in the  $A$  component, the north is up and the east is to the left. Two red points correspond to the moments when the radial velocity of the components (presented in Table 7) was measured – see text for details.

for ZZ Tau between JD 2 430 360.5 and 2 430 725.0 were in the range  $14^m 75 - 15^m 0$ .

As can be seen from the figure the average brightness of ZZ Tau in the  $B$  band smoothly decreased till the beginning of 1950s and then began to increase, but the amplitude of variability significantly decreased. We can not say anything about the behaviour of the star in the  $V$  band before 1942 due to the absence of data, but note that the *average*  $V$  magnitude of ZZ Tau was nearly constant in the second half

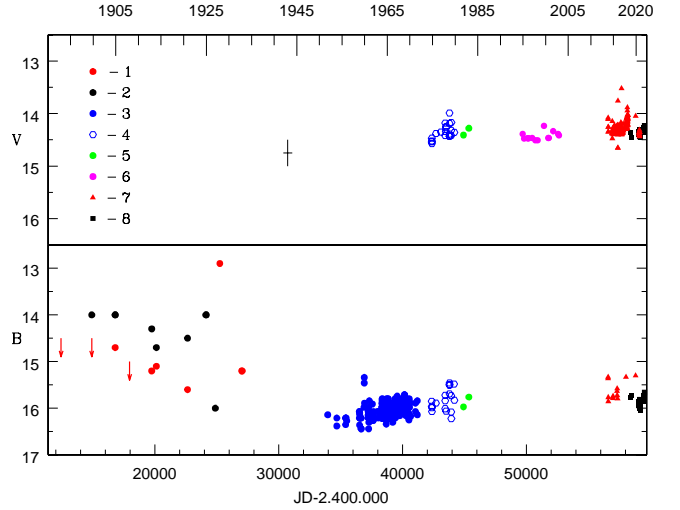


**Figure 3.** The historical light curve of ZZ Tau AB in the  $V$  (upper panel) and  $B$  (low panel) bands. Symbols of different colour and/or shape correspond to different data sources: 1 – Reinmuth (1930), 2 – Himpel (1944), 3 – Malyshev (1972), 4 – Nurmanova (1983), 5 – Rydgren & Vrba (1983), 6 – Schaefer et al. (2003), 7 – AAVSO, 8 – this work.

of the 20th century: e.g., compare  $14^m 34$  from Herbig & Bell (1988),  $14^m 35$  from Kenyon & Hartmann (1995) with our  $14^m 38$  in 2020 (see Fig. 5).

A more detailed light curve based on our observations only is presented in Fig. 4. It can be seen that the binary becomes brighter in all the bands in 2021 than in 2020, and to a greater extent in the short-wavelength region. We will discuss this feature in Sect. 3.4.

Rodriguez et al. (2017) found periodical brightness variations of ZZ Tau A+B from ground based observations and attributed them to rotation modulation with the period  $P_{\text{rot}} = 1^d 311$ . Rebull et al. (2020) did not confirm this period from the analysis of the space K2 data, but found another period  $P_{\text{rot}} = 4^d 1609$ . Based on our data we found the following values  $4^d 1688$ ,  $4^d 1702$  and  $4^d 1739$ , for the  $V$ ,  $R$  and  $I$  bands, respectively. The average value  $P_{\text{rot}} = 4^d 1710 \pm 0^d 0022$  is close to the result obtained by Rebull et al. (2020). The shorter period  $1^d 311$  is the one day alias of the real one.

The phase curves in different optical bands as well as  $B - V$ ,  $V - R$  and  $V - I$  colours are shown in Fig. 5. It can be seen from the left column of the figure, that the less the effective wavelength of the photometric band the more blurred becomes the phase curve, and in the  $U$  band the periodicity disappears. We will discuss this feature in Sect. 3.4. The periodicity is only marginally seen in the colours, prob-

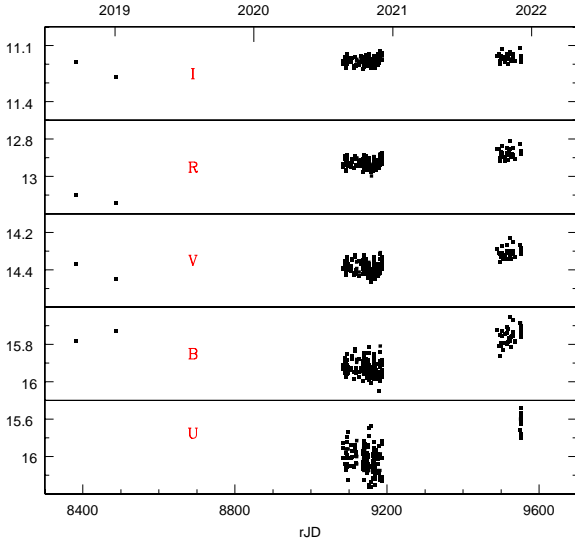


**Figure 4.** The *UBVRI* light curves of ZZ Tau A+B based on our data from Table 1 only. Note that the binary is brighter in the second half of the 2021 season than in 2020.

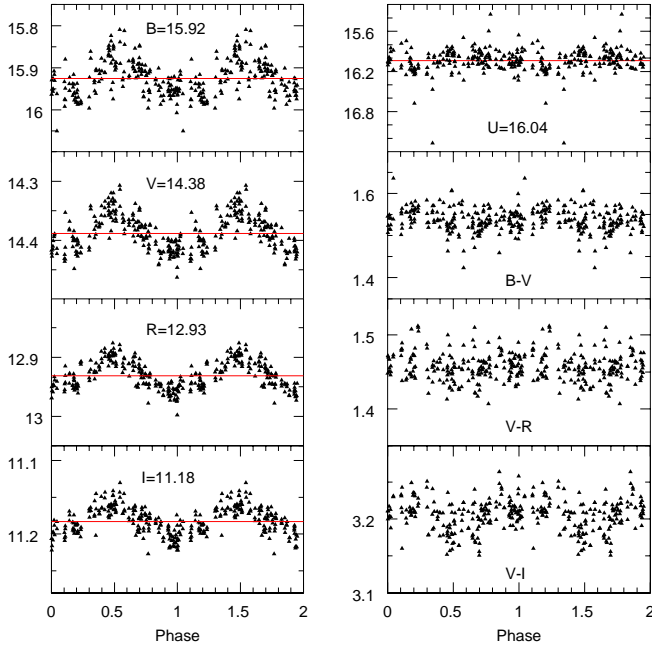


**Figure 5.** The *UBVRI* and colours phase curves of ZZ Tau corresponding to the period  $P \approx 4^d.17$ , based on the data from Tabl. 1. The average brightness of the binary in each band is shown by a red line in respective panels. Note that periodicity is clearly seen in the panels of the left column in contrast to those of the right one.

ably because the amplitude of the variability is comparable to the errors of measurements.

As follows from Table 2 the *J* and *H* magnitudes of ZZ Tau A+B were constant during our observations within errors of measurements ( $\bar{J} = 9^m.42$ ,  $\bar{H} = 8^m.74$ ), and small variability with an amplitude of  $\approx 0^m.03$  can be suspected in the *K* band ( $\bar{K} = 8^m.42$ ). One can compare these results with previous NIR observations: for example  $J = 9.52 \pm 0.02$ ,

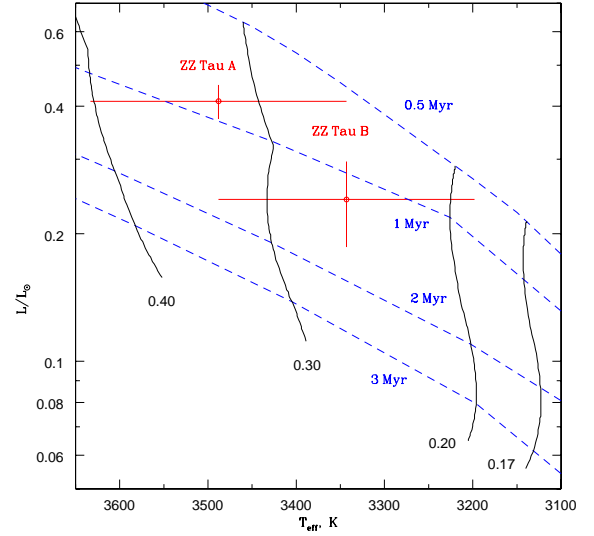


**Figure 6.** The position of ZZ Tau A and ZZ Tau B on Hertzsprung-Russel diagram. The evolutionary tracks (solid lines) and isochrones (dashed lines) adopted from Baraffe et al. (2015) are also plotted.

$H = 8.78 \pm 0.02$ ,  $K = 8.54 \pm 0.02$  (Rydgren & Vrba 1983) or  $J = 9.46 \pm 0.02$ ,  $H = 8.72 \pm 0.02$ ,  $K = 8.51 \pm 0.02$  (Whitney et al. 1997).

### 3.3 Parameters of ZZ Tau’s components

Based on spatially resolved IR spectra of the binary Schaefer et al. (2014) found the effective temperature  $T_{\text{eff}}$ , extinction  $A_V$  and bolometric luminosity  $L_{\text{bol}}$  for each component. We have no such spectra, so we have to use the results of these authors hereinafter:  $T_{\text{eff}}^A = 3488 \pm 145$  K,  $L_{\text{bol}}^A = 0.411 \pm 0.038 L_{\odot}$  and  $T_{\text{eff}}^B = 3343 \pm 145$  K,  $L_{\text{bol}}^B = 0.241 \pm 0.055 L_{\odot}$ . Then the radii of the components are  $R^A \approx 1.76 \pm 0.17$  and  $R^B \approx 1.47 \pm 0.21 R_{\odot}$ .

To estimate the age and mass of the binary components Schaefer et al. (2014) used theoretical tracks and isochrones of Baraffe et al. (1998); Siess et al. (2000); Dotter et al. (2008); Tognelli et al. (2011). It was found that the age of the system is  $< 3$  Myr and ‘for all sets of tracks, the sum of the evolutionary masses of the components agrees at the  $1\sigma$  level with the total dynamical mass’  $M_{A+B} = 0.83 \pm 0.16 M_{\odot}$ .

We also plot the positions of ZZ Tau’s components in the Hertzsprung-Russel diagram (see Fig. 6), but use more recent theoretical calculations of Baraffe et al. (2015). It follows from the plot that the mass of the primary is  $M_A = 0.33 \pm 0.08 M_{\odot}$  and that of the secondary is  $M_B = 0.26 \pm 0.06 M_{\odot}$ . Thus, the total mass of the binary  $M_{A+B}$  is  $0.59 \pm 0.10 M_{\odot}$ , that is somewhat less than the mass derived from our orbital solution:  $0.86 \pm 0.09 M_{\odot}$ . This discrepancy will disappear if the actual distance  $d$  to the star is 5-10 % less than the accepted value of 140 pc, because the dynamical mass is proportional to  $d^3$ . Cold and hot spots on the surfaces of ZZ Tau’s components (see the next section) can also alter the estimation of their  $T_{\text{eff}}$  and ‘the inferred stellar masses from stellar evolutionary models’ (Flores et al.

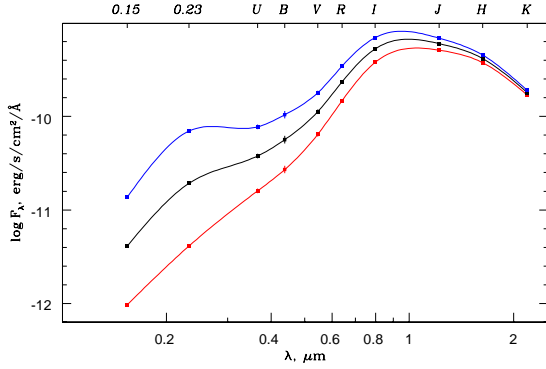


**Figure 7.** The spectral energy distribution of ZZ Tau A+B based on our and GALEX (Gómez de Castro et al. 2015) broad band photometric data (squares): observed (red) and dereddened with  $A_V = 0.6$  (black) and 1.1 (blue), respectively. The curves are spline interpolations of the data and are drawn for clarity. See text for details.

2022). As follows from the figure the age of the system is between 0.5 and 2 Myr.

The luminosities and radii of the components depend on the extinction adopted by Schaefer et al. (2014):  $A_V^A = 1.49 \pm 0.34$ ,  $A_V^B = 1.24 \pm 0.87$ . At the same time  $A_V^{A+B}$  found by Herczeg & Hillenbrand (2014) from spatially unresolved spectra of ZZ Tau A+B is significantly less:  $0.55 \pm 0.1$ . Spectral energy distribution of ZZ Tau A+B based on our and GALEX (Gómez de Castro et al. 2015) broad band photometric data (Fig.7) also indicate that the situation with extinction is not clear.

To convert the  $UBVR IJHK$  and  $FUV$ ,  $NUV$  magnitudes to monochromatic fluxes  $F_\lambda$  we used the constants from the papers of Bessell et al. (1998) and Morrissey et al. (2007), respectively. Then we dereddened observed fluxes assuming the standard extinction law with  $R_V = 3.1$  (Cardelli et al. 1989). As follows from the figure the  $F_\lambda(\lambda)$  dependence has a maximum shortward of the  $U$  band for  $A_V > 1$ . But if the observed UV emission of ZZ Tau A+B is connected with an accretion spot (see the next section), then the accretion shock theory predicts (Lamzin 1995; Calvet & Gullbring 1998; Dodin 2018) that the flux shortward of  $\lambda = 0.36 \mu\text{m}$  should decrease with decreasing wavelength. For this reason, we believe that the appearance of the maximum in the  $F_\lambda(\lambda)$  curve is the result of excess dereddening which occurs due to the presence of a local maximum (bump) in the extinction curve  $A_\lambda(\lambda)$  at  $\lambda \approx 0.22 \mu\text{m}$ .

If so, then  $A_V$  should be  $< 1.0$ , however this statement is based on the assumption that the continuum rather than line emission (e.g. C IV 1550 and Mg II 2800 doublets) is the main sources of radiation in FUV and NUV GALEX’s spectral bands. Future spectral observations of ZZ Tau in the UV band – e.g. with WSO-UV (Boyarchuk et al. 2016) – will make it possible to find out if this is the case. X-ray observations of the binary will also help to clarify  $A_V$ .

According to Schaefer et al. (2014)  $A_V^A > A_V^B$  but the difference of these values is less than  $1\sigma$ , so it well can be that the extinction is the same for the primary and the secondary. Note however that shortward of  $\lambda \approx 0.6 \text{ nm}$  the flux of ZZ Tau A decreases faster than that of ZZ Tau B with the wavelength decreasing (see Fig.1), although it should be the

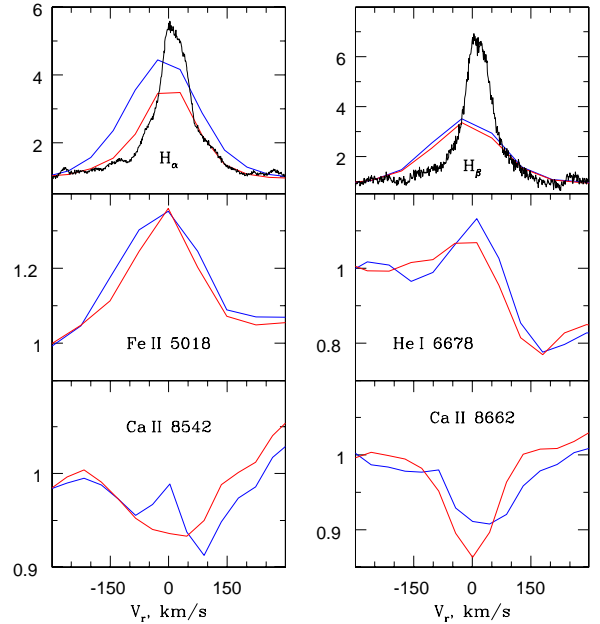


**Figure 8.** The relative intensities of the most prominent lines in the MUSE spectrum of ZZ Tau A and ZZ Tau B (blue and red curves, respectively). The UVES-1 spectrum of ZZ Tau A+B is shown in upper panels for comparison (black curves). The profiles in each panel are normalised to the nearby continuum level. The heliocentric radial velocity is plotted along the horizontal axis.

opposite, since the effective temperature of the companion is less than that of the primary. A smaller extinction in the direction to ZZ Tau B could eliminate this discrepancy.

### 3.4 The nature of the component’s activity

We have identified a number of emission lines in the ZZ Tau A+B spectra – see Figs.8–10. Among the most prominent are the Balmer lines of hydrogen (from  $H\alpha$  to at least  $H\delta$ ), He I (triplet  $\lambda\lambda$  4471.5, 5875.6 and singlet  $\lambda$  4921.9, 5015.7, 6678.2 Å), Ca II (H, K, IR triplet), Mg I  $\lambda\lambda$  5167.3, 5172.7 Å lines as well as the strongest lines of Fe I ( $a^3F - z^3D^o$ ,  $a^3F - z^3F^o$ ,  $a^3F - z^3D^o$ ) and Fe II ( $a^6S - z^6P^o$ ,  $a^4G - z^4F^o$ ) multiplets. All the iron lines have  $\log(gf) > -1.9$ , and an excitation energy of the low level is  $E_i \lesssim 3.3 \text{ eV}$ .

As can be seen from Fig.1 and 8 the emission lines are present in the spectra of both components. In particular, the  $H\alpha$  equivalent width is  $22 \pm 1$  and  $13 \pm 0.5 \text{ \AA}$  in the MUSE spectra of ZZ Tau A and B, and that of  $H\beta$  is  $\approx 13$  and  $11 \text{ \AA}$ , respectively. Observed secondary to primary  $H\alpha$  flux ratio in the MUSE spectra is 0.30 and  $H\beta$  flux ratio is 0.71. It means that the relative contribution of ZZ Tau B to the  $H\alpha$  and  $H\beta$  fluxes in the total ZZ Tau A+B spectra are  $\sim 20$  and 40%, respectively.

In Fig. 9 we compared the profiles of some H I, He I and Fe II emission lines from the high resolution spectra of ZZ Tau A+B observed in 2008-2010 (left panel) and 2018 November-December. It can be seen that the profiles and EWs of these lines are variable. In particular, the EW of  $H\alpha$  varied between 8.8 to 17 Å in the 2008-2010 spectra, and between 8.5 and 9.4 Å in the 2018 UVES spectra. But the

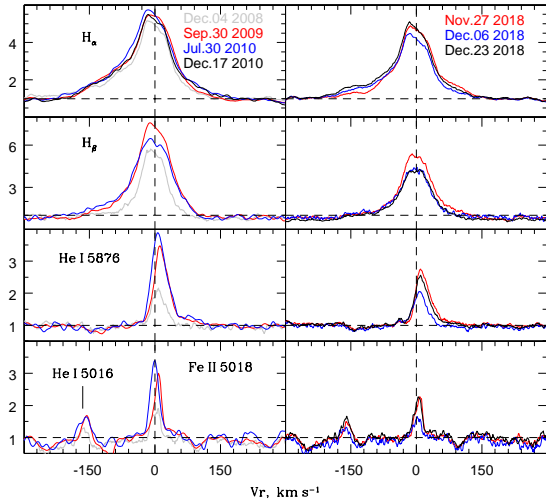


**Figure 9.** The profiles of some emission lines in the 2008-2010 (left column) and 2018 (right column) spectra of ZZ Tau A+B. According to Table 4, the spectra from the right column corresponding to dates 2018-Nov-27, 2018-Dec-07 and 2018-Dec-24 are referred to in the text as the abbreviation UVES-1, UVES-2 and UVES-3, respectively. The profiles are plotted in stellar rest frame assuming  $V_r \approx 17.3 \text{ km s}^{-1}$  for the left panel and  $15.4 \text{ km s}^{-1}$  for the right one.

profiles of the same lines in both panels have not changed qualitatively, so it seems reasonable to compare the short term line profile variability with periodical photometric variability.

According to Table 4 the phase differences between the moments of obtaining the UVES-2 and UVES-3 spectra relative to that of the UVES-1 one are  $\approx 2.39 \pm 0.005$  and  $6.42 \pm 0.01$ , respectively, for the rotation period  $P_{\text{rot}} = 4^d 171 \pm 0.002$ . If the observed line variability is related to the rotational modulation, then one can expect that the line profiles should be nearly identical in the UVES-2 and UVES-3 spectra and differ from those in the UVES-1 spectrum. But as can be seen from the right panel of Fig. 9 this is true only for the  $H\beta$  line, and for all other lines the situation is quite the opposite: the profiles in the UVES-2 and UVES-3 spectra differ significantly, but are more or less similar in the UVES-1 and UVES-2 spectra. This can be seen even more clearly in the case of the Fe I  $a^5F - z^5D^o$  multiplet lines shown in Fig. 10. We will try to explain this discrepancy (the ‘phase problem’) a bit later.

The He I and Fe II emission lines in Fig. 9 as well as the emission components of Fe I lines in Fig. 10 are redshifted. Using our orbital parameters one can find that at the middle epoch of the UVES spectra observations (the beginning of December 2018) the true anomaly  $v$  was  $\approx 181^\circ$ . Then, according to Eq.(1), the difference of the component’s radial velocities  $V_r^B - V_r^A$  was  $\approx -1.6 \text{ km s}^{-1}$  at that moment in the case of the ‘mirror’ orbit. As can be seen from the figures, the maximum of He I, Fe I and Fe II line profiles in the UVES spectra are redshifted greater – from 5 to  $10 \text{ km s}^{-1}$ . Probably it means that they are really redshifted in the spectra of the primary, but it is not so obvious in the case of ZZ Tau B. The situation with the emission components of the infrared Ca II triplet lines in the ZZ Tau A+B spectra (see Fig. 11), is similar: their profiles are also variable and slightly red-

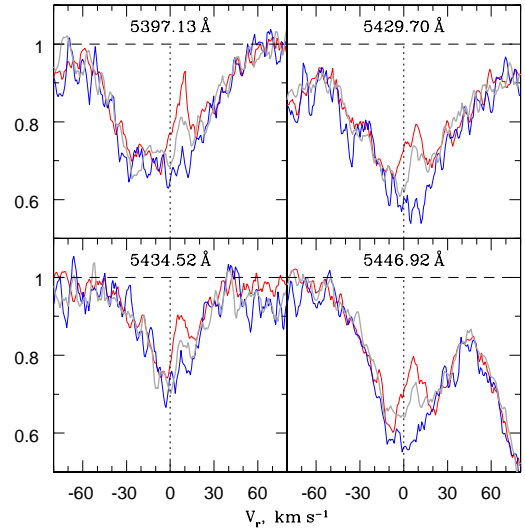


**Figure 10.** The profiles of some Fe I  $a^5F - z^5D^o$  multiplet lines in the 2018 November 27 (UVES-1, red), December 06 (UVES-2, blue) and December 23 (UVES-3, gray) spectra of ZZ Tau A+B. The radial velocity along the abscissa axis refers to the rest frame of the star.

shifted. Unfortunately, the spectral resolution of the MUSE spectrum is too low to detect the redshift of emission lines for each component which is of the order of several  $\text{km s}^{-1}$ .

The average  $H\alpha$  line flux in the three UVES ZZ Tau A+B spectra is  $\approx 1.3 \times 10^{-13} \text{ erg s}^{-1} \text{ cm}^{-2}$ . If we suppose that this value stayed constant during the MUSE spectral observations (one year later) and use the component’s flux ratio mentioned above, we can find the observed as well as de-reddened (Cardelli et al. 1989)  $H\alpha$  line flux  $F_{H\alpha}$  of each component of the binary, and their respective luminosities  $L_{H\alpha} = 4\pi d^2 F_{H\alpha}$ , where  $d = 140 \text{ pc}$  is the distance to ZZ Tau. Thus, we found  $L_{H\alpha}^A \approx 7.3 \times 10^{29} \text{ erg s}^{-1}$  and  $L_{H\alpha}^B \approx 1.8 \times 10^{29} \text{ erg s}^{-1}$ .

To estimate the accretion luminosity  $L_{\text{acc}}^A$  of ZZ Tau A we used the statistical relation

$$\log \left( \frac{L_{\text{acc}}}{L_{\odot}} \right) = 1.13 \log \left( \frac{L_{H\alpha}}{L_{\odot}} \right) + 1.74 \quad (3)$$

of Alcalá et al. (2017) and found that  $L_{\text{acc}}^A \approx 1.3 \times 10^{31} \text{ erg s}^{-1}$ . Then we estimated the ZZ Tau A’s accretion rate from Eq.1 of Alcalá et al. (2017) and found  $\dot{M}_{\text{acc}}^A \sim 7 \times 10^{-10} M_{\odot} \text{ yr}^{-1}$ . Applying the same procedure to ZZ Tau B leads to a four time less  $\dot{M}_{\text{acc}}^B$ .

As follows from Fig. B.1 of Alcalá et al. (2017) both components of the binary are located in the region of the  $\log L_{\text{acc}}$  vs  $T_{\text{eff}}$  diagram where the chromospheric contribution to the line emission is negligible. Thus, it seems reasonable to conclude that accretion rather than chromospheric activity is responsible for the line emission observed in both components of ZZ Tau. Recall also that Espaillet et al. (2012) concluded that at least one component of the binary has an optically thick accretion disc.

Our value of  $\dot{M}_{\text{acc}}^A + \dot{M}_{\text{acc}}^B$  is between the accretion rates found by Cieza et al. (2012) and Valenti et al. (1993) from spatially unresolved ZZ Tau A+B’s spectra. Note however that Eq. 3 is statistical in its nature, so our estimate of  $\dot{M}_{\text{acc}}$  is valid up to a factor of 2-3. A more accurate estimation can

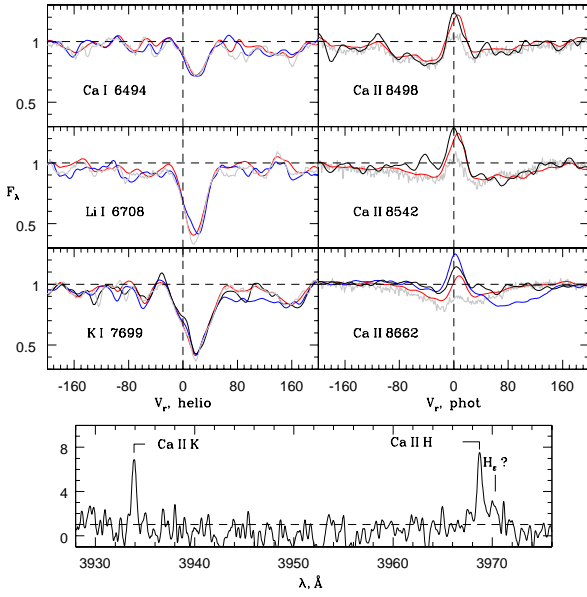


**Figure 11.** The profiles of some lines in the 2008 Dec.04 (grey), 2009 Sep.30 (red), 2010 Jul.30 (blue) and 2010 Dec.17 (black) spectra of ZZ Tau A+B. Left column – the absorption lines in heliocentric frame, right column – the Ca II infrared triplet lines in the stellar rest frame assuming  $V_r \approx 17 \text{ km s}^{-1}$ . A portion of ZZ Tau spectrum averaged over all the 2009-2010 observations and additionally smoothed with a running average over 10 points is shown in the middle bottom panel.

be found via a respective analysis of a series of high resolution spectra of each component of the binary (Dodin et al. 2013). Nevertheless, if our estimate is correct to the order of magnitude, then the time for the circumprimary disc to exhaust its matter is  $M_{\text{disc}}/\dot{M}_{\text{acc}}^A < 3 \times 10^5 \text{ yr}$ , i.e. significantly less than the age of the binary. So, one can expect that there is a matter flow from the CB disc at least to the disc of the primary.

Let’s get back to the ‘phase problem’ now, assuming that the observed photometric periodicity results from the rotational modulation of the accretion hot spot continuum emission. We have mentioned in Sect. 3.2 (see Fig. 5) that the  $4^{\text{d}}17$  phase curve is clearly seen in the  $V$ ,  $R$ ,  $I$  bands, becomes blurred in the  $B$  band and that the periodicity is not seen in the  $U$  band. At the same time the relative contribution of ZZ Tau B to the total flux of ZZ Tau A+B begins to increase with wavelength decreasing at  $\lambda \lesssim 0.6 \mu\text{m}$  (see Fig. 1), so we believe that the emission of ZZ Tau B is much stronger in the  $U$  band than that of the primary. One can explain these facts if the accretion hot spot responsible for the observed photometric periodicity is located on ZZ Tau A.

On the other hand, we could not reliably detect the periodicity in the  $U$  band, where presumably ZZ Tau B is the main source of emission.<sup>9</sup>

It could be due e.g. to the angle between the rotational and magnetic axes of the secondary being  $\lesssim 30^\circ$  and the accretion flow being divided into several unstable ‘tongues’

<sup>9</sup> More precisely we found the period  $P = 2^{\text{d}}237$ , but its false alarm probability is  $\approx 10 \%$ , i.e. large enough. Moreover this value of  $P$  does not solve the ‘phase problem’.

that produce chaotic hot spots on the stellar surface resulting in an irregular light curve – see Romanova et al. (2021) and references therein. If so, one can explain the ‘phase problem’ in the following way.

As was noted, the contribution of the secondary to the total radiation of ZZ Tau A+B is approximately the same in line and continuum emission and varies from 20 to 40 % in the range from 0.5 to 0.9  $\mu\text{m}$ . This is enough to noticeably affect the shape of the lines in the total spectrum of the binary, and to increase the noise level of the photometric phase curve, and the effect is the greater, the greater relative flux contribution of the companion. And where the radiation of ZZ Tau B dominates (e.g. in the  $U$  band) photometric periodicity disappears.

It was mentioned in Sect.3.2 that the binary became brighter in all the bands in 2021 than in 2020, and to a greater extent in the short-wavelength region (Fig. 4).<sup>10</sup> The amplitude of photometric variability in the historical light curve is also significantly larger in the  $B$  than  $V$  band (Fig.3). This suggests that the secondary rather than the primary is responsible for the long term photometric variability of ZZ Tau. The chaotic accretion regime (Kulkarni & Romanova 2008) may be responsible for an increased photometric activity of ZZ Tau B. Note in this regard that there is no obvious relation between the historical light curve and relative position of the binary components.

It’s especially worth mentioning that we did not find any gas outflow signs in the spectra of ZZ Tau A+B: there are neither forbidden lines nor clear excess emission in blue wings of permitted lines which is in agreement with the observations of other authors (Valenti et al. 1993; Kenyon et al. 1998; Folha & Emerson 2001; Herczeg & Hillenbrand 2014).

At the end of this section we would like to draw attention to the following. As was demonstrated above, the variable redshifted emission component is present in the red wing of Fe I lines, no matter which component of the binary they are related to. It well can be that other absorption lines also have similar (but not so strong) variable redshifted emission, as a result of which the centroid of the lines will be shifted, and this ultimately leads to an error in determining the radial velocity of the companion or the primary (Dodin et al. 2013). The discrepancies in the calculated and observed radial velocities of ZZ Tau’s components (see Table 7) may be partly due to this effect.

#### 4 CIRCUMSTELLAR ENVIRONMENT OF THE BINARY

As was noted above there are no indications of matter outflow in the optical and near IR spectra of ZZ Tau A+B, but there is a monopolar redshifted  $^{12}\text{CO}$  molecular outflow in the vicinity of the binary (Heyer et al. 1987). In the left panel of Fig. 12 we reproduce a portion of Fig.27 of Narayanan et al. (2012), who analysed the velocity field of

<sup>10</sup> The accuracy of our speckle interferometric measurements is not enough to determine, which component of the binary has become brighter: as we noted in Sect. 2 the difference of component’s relative brightness in 2020 and 2021 observational seasons at  $\lambda \approx 0.9 \mu\text{m}$  is less than the errors of measurements.

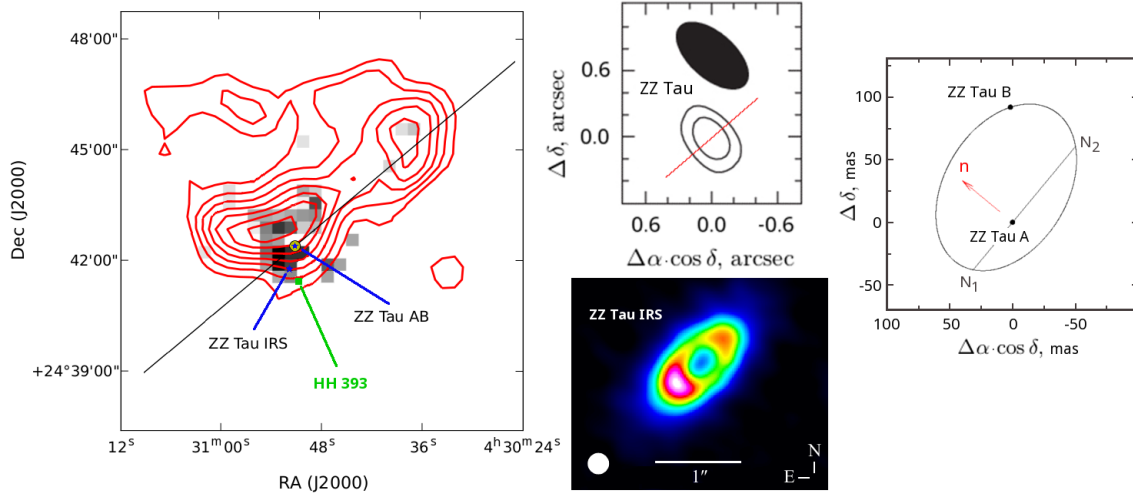


**Figure 12.** Left panel – a monopolar redshifted CO molecular outflow of ZZ Tau (red isophotes) and its axis (black line) according to Narayanan et al. (2012). The positions of ZZ Tau IRS and HH393 are also shown. Middle panels: top – the isophotes of ZZ Tau’s CB disc (solid lines) and the corresponding beam size (Akeson et al. 2019); bottom – the protoplanetary disc of ZZ Tau IRS (Hashimoto et al. 2021). The red line is the direction of the CO outflow. Right panel – the relative orbit of ZZ Tau binary shown for comparison.  $N_1$ – $N_2$  is a node line, and  $n$  is the projection of orbital momentum vector to the sky. See text for details.

the outflow and concluded that the position angle of its axis is  $PA_{CO} \approx 130^\circ$  – see the black line in the panel. Narayanan et al. (2012) noted that it is not possible to decide whether ZZ Tau or ZZ Tau IRS is the source of the outflow, relying only on its morphology.

To solve the problem one can try to use information about orientation of protoplanetary discs of these objects assuming that the outflow axis is perpendicular to the disc plane. In this case the axis of the CO-outflow should be oriented along the minor axis of ALMA image of (presumably round shape) respective disc. Unfortunately, the continuum CB disc of ZZ Tau measured by Akeson et al. (2019) appears to be smaller than the beam size and therefore unresolved – see the upper middle panel of Fig. 12. By contrast, the circumstellar disc of ZZ Tau IRS is fully resolved (see the middle bottom panel of Fig. 12) and the position angle of its minor axis is  $45^\circ$  (Hashimoto et al. 2021). It means that the minor axis of ZZ Tau IRS disc is almost perpendicular to the axis of CO outflow and pointing almost to the Herbig-Haro object HH393. On this basis, we believe that ZZ Tau binary is the source of the CO-outflow, but ZZ Tau IRS is the source of HH393 outflow.

Additional more sensitive and with better angular resolution ALMA observations of ZZ Tau’s CB disc are needed to determine its inclination  $i_d$  and the position angle of the disc’s ascending node  $\Omega_d$ . It will then be possible to determine the inclination  $\Theta$  of ZZ Tau A+B’s orbital plane to the CB disc of the binary as follows. The projection of the angular momentum unit length vectors of the disc  $\mathbf{n}_d$  and orbital motion  $\mathbf{n}_o$  in our coordinate system (see the footnote to Sect. 3.1) is:  $\{\cos i_j \cos \Omega_j; \sin i_j \sin \Omega_j; \cos i_j\}$ , where  $j = d$  and  $o$ , respectively. Then, the angle  $\Theta$  between the  $\mathbf{n}_d$  and  $\mathbf{n}_o$  vectors can be found from their scalar product:

$$\cos \Theta = \cos i_d \cos i_o + \sin i_d \sin i_o \cos(\Omega_d - \Omega_o). \quad (4)$$

As far as we have proposed that the observed periodic brightness variations of ZZ Tau in the *BVRI* bands are related to axial rotation of the primary, then one can esti-

mate the inclination  $i_*$  of its axis to the line of sight from the relation:

$$\sin i_* = \frac{P_{\text{rot}} \times v \sin i}{2\pi R}. \quad (5)$$

According to L. Prato (private communication) the projected rotational velocities  $v \sin i$  of ZZ Tau A and ZZ Tau B are  $11 \pm 1$  and  $17 \pm 1$   $\text{km s}^{-1}$ , respectively.<sup>11</sup> It means that the axis of ZZ Tau A is inclined to the line of sight at  $\approx 31^\circ \pm 4^\circ$ .

The absence of detectable blueshifted CO emission near ZZ Tau (see the left panel of Fig. 12) implies a small amount of cold gas (the remnants of the parent protostellar cloud) in front of the binary. The polarization of ZZ Tau’s radiation (see Table 3) is also small ( $p_I \approx 0.27\%$ ) and stable. It can be explained by interstellar dichroic absorption. Taking into account the Serkowski law determined for Elias 9 (Whittet et al. 1992), which is  $0^\circ.317$  away from ZZ Tau,  $p_V$  for ZZ Tau should be  $\approx 0.12\%$ , that corresponds to the interstellar  $A_V \gtrsim 0.04$ . Thus, we concluded that a relatively large extinction in the direction to the components of the binary ( $A_V^A \approx 1.5$  and  $A_V^B \approx 1.2$  according to Schaefer et al. (2014)) is related to the matter in the immediate vicinity of these stars. Recall in this connection that the matter flow from the CB disc to the disc of ZZ Tau A can still continue.

## 5 SUMMARY

The results of our investigation of ZZ Tau can be summarized as follows.

(i) We clarified the orbital parameters of the binary using published and our new astrometric observations. It appeared that our parameters differ from those of Schaefer et al. (2014) by  $< 1\sigma$ , but have 1.5 – 2 times better accuracy.

<sup>11</sup> López-Valdivia et al. (2021) and Nofi et al. (2021) reported  $v \sin i = 20.6 \pm 2$  and  $18.4 \pm 2.4$   $\text{km s}^{-1}$ , respectively for ZZ Tau A+B.

(ii) According to our calculations, the parameters of the binary are: the orbital period of the binary  $P = 46.8 \pm 0.8$  yr, semimajor axis  $a = 12.35 \pm 0.29$  au, eccentricity  $e = 0.58 \pm 0.02$ , inclination of the orbit  $i = 123^\circ.8 \pm 1^\circ.0$ , and total mass of the binary  $0.86 \pm 0.09 M_\odot$ . In particular, this means that the minimal distance between the components is  $\approx 5.2$  au.

(iii) It is not possible to determine the direction of the ascending node from a visual orbit alone, so the two solutions with  $(\omega, \Omega)$  and  $(\omega + 180^\circ, \Omega + 180^\circ)$  are equivalent from a visual binary perspective. We used the radial velocities to break the degeneracy between these two solutions and determine the direction of the ascending node. But it is a preliminary conclusion, because it appeared that a variable emission component can present in the red wing of (at least some) absorption lines, thus introducing an error to the companion's radial velocity measurements. High resolution spatially resolved spectra of ZZ Tau's components are required to take this effect into account.

(iv) The radiation of ZZ Tau B dominates shortward of  $\lambda \approx 0.4 \mu\text{m}$  in the SED of ZZ Tau A+B, despite the fact that  $T_{\text{eff}}^{\text{B}} < T_{\text{eff}}^{\text{A}}$ . In our opinion, this means that the extinction in the direction to the primary is larger than to the secondary presumably due to an excess amount of circumstellar material in the vicinity of ZZ Tau A.

(v) We found that the rotation axis of the primary is inclined to the line of sight by  $\approx 31^\circ \pm 4^\circ$ .

(vi) Using the isochrones of Baraffe et al. (2015), we conclude that the age of both ZZ Tau's components is between 0.5 and 2 Myr.

(vii) The emission lines are observed in the spectra of both ZZ Tau's components, e.g. the equivalent width of H $\alpha$  line in the MUSE spectra of ZZ Tau A and B is  $\approx 22$  and  $13 \text{ \AA}$ , respectively. We concluded that the observed line as well as the continuum excess emission in the spectra of both components is due to accretion of disc matter. According to our estimate, the accretion rate to the primary is  $\dot{M}_{\text{acc}}^{\text{A}} \sim 7 \times 10^{-10} M_\odot \text{ yr}^{-1}$  and  $\approx 4$  times less in the case of ZZ Tau B.

(viii) The periodical light variations of ZZ Tau A+B with a period of  $P = 4^{\text{d}}1710 \pm 0^{\text{d}}0022$  were observed in the *BVRI* bands that is close to the period of  $4^{\text{d}}1609$  reported by Rebull et al. (2020). It follows from our data that the period  $1^{\text{d}}311$  (Rodríguez et al. 2017) is probably the one day alias of the real one. We believe that the periodicity is related to axial rotation of an accretion (hot) spot on the surface of the primary.

(ix) We did not observe a  $4^{\text{d}}17$  periodicity in the *U* band or in the variations of emission line profiles presumably due to a significant contribution of the ZZ Tau B emission.

(x) There is no obvious correlation between long-term photometric variability of ZZ Tau and orbital position of the binary components. We believe that ZZ Tau B is responsible for the large amplitude photometric variability of the binary observed in the first half of the last century.

(xi) Judging by the orientation of ZZ Tau IRS's disc, it seems much more likely that ZZ Tau A+B is the source of CO-molecular outflow but ZZ Tau IRS is the source of Herbig-Haro object HH393.

Apparently our estimation of the binary orbital parameters is reliable enough. It is necessary to obtain high resolution optical spectra of each component at different phases of rotation period to get more reliable estimates of the com-

ponent's parameters (effective temperatures, extinction(s), luminosities, radii, and accretion rates). We also propose to include ZZ Tau in the target list of spectral UV observations with WSO-UV space mission (Boyarchuk et al. 2016). Additional more sensitive and with better angular resolution ALMA observations of ZZ Tau are highly desirable to get important information on the parameters of its CB disc. We hope that these new observations will help to clarify whether the extinction in the direction of the binary components is different and to understand the reason for the increased photometric activity of ZZ Tau in the first half of the last century.

## ACKNOWLEDGEMENTS

We thank the staff of the Caucasian Mountain Observatory headed by N. Shatsky for the help with observations as well as Regina von Berlepsch and Matthias Steffen for sending us a copy of the Himpel (1944) paper. We also thank N.N. Samus and L.M. Rebull for useful discussions and especially Dr. L. Prato who has sent us the unpublished results of  $V_r$  and  $v \sin i$  measurements for the ZZ Tau components. We give our special thanks to the anonymous reviewer for the comments made, which allowed us to eliminate shortcomings and inaccuracies presented in the original version of the paper. We acknowledge with thanks the variable star observations from the AAVSO International Database contributed by observers worldwide and used in this research. This research has made use of the SIMBAD database, operated at CDS, Strasbourg, France. The study of AD (observations, data reduction, interpretation) and SL (interpretation) and BS (polarimetric observations and data reduction) was conducted under the financial support of the Russian Science Foundation 17-12-01241.

The acquisition of scientific equipment used in this study was partially supported by the M. V. Lomonosov Moscow State University Program of Development.

## DATA AVAILABILITY

The photometric data used in this article are available in online supplementary material. Other data used in this article will be shared on reasonable request to the corresponding author.

## References

- Akeson R. L., Jensen E. L. N., Carpenter J., Ricci L., Laos S., Nogueira N. F., Suen-Lewis E. M., 2019, *ApJ*, **872**, 158
- Alcalá J. M., et al., 2017, *A&A*, **600**, A20
- Andrews S. M., Williams J. P., 2005, *ApJ*, **631**, 1134
- Andrews S. M., Rosenfeld K. A., Kraus A. L., Wilner D. J., 2013, *ApJ*, **771**, 129
- Artymowicz P., Lubow S. H., 1994, *ApJ*, **421**, 651
- Audard M., Briggs K. R., Grosso N., Güdel M., Scelsi L., Bouvier J., Telleschi A., 2007, *A&A*, **468**, 379
- Bally J., Walawender J., Reipurth B., 2012, *AJ*, **144**, 143
- Baraffe I., Chabrier G., Allard F., Hauschildt P. H., 1998, *A&A*, **337**, 403
- Baraffe I., Homeier D., Allard F., Chabrier G., 2015, *A&A*, **577**, A42

- Bate M. R., 2018, *MNRAS*, **475**, 5618
- Bate M. R., Lodato G., Pringle J. E., 2010, *MNRAS*, **401**, 1505
- Berdnikov L. N., Belinskii A. A., Shatskii N. I., Burlak M. A., Ikonnikova N. P., Mishin E. O., Cheryasov D. V., Zhuiko S. V., 2020, *Astronomy Reports*, **64**, 310
- Bessell M. S., Castelli F., Plez B., 1998, *A&A*, **333**, 231
- Boyarchuk A. A., et al., 2016, *Astronomy Reports*, **60**, 1
- Calvet N., Gullbring E., 1998, *ApJ*, **509**, 802
- Cardelli J. A., Clayton G. C., Mathis J. S., 1989, *ApJ*, **345**, 245
- Cieza L. A., Schreiber M. R., Romero G. A., Williams J. P., Rebassa-Mansergas A., Merín B., 2012, *ApJ*, **750**, 157
- Dodin A., 2018, *MNRAS*, **475**, 4367
- Dodin A. V., Lamzin S. A., Sitnova T. M., 2013, *Astronomy Letters*, **39**, 315
- Dodin A., et al., 2019, *MNRAS*, **482**, 5524
- Doppmann G. W., Najita J. R., Carr J. S., 2017, *ApJ*, **836**, 242
- Dotter A., Chaboyer B., Jevremović D., Kostov V., Baron E., Ferguson J. W., 2008, *ApJS*, **178**, 89
- Emeyanov N., 2020, The Dynamics of Natural Satellites of the Planets
- Espaillet C., et al., 2012, *ApJ*, **747**, 103
- Flores C., Connelley M. S., Reipurth B., Duchêne G., 2022, *ApJ*, **925**, 21
- Folha D. F. M., Emerson J. P., 2001, *A&A*, **365**, 90
- Furlan E., et al., 2011, *ApJS*, **195**, 3
- Gaia Collaboration et al., 2016, *A&A*, **595**, A1
- Gaia Collaboration Brown A. G. A., Vallenari A., Prusti T., de Bruijne J. H. J., Babusiaux C., Biermann M., 2020, arXiv e-prints, p. [arXiv:2012.01533](https://arxiv.org/abs/2012.01533)
- Gómez de Castro A. I., Lopez-Santiago J., López-Martínez F., Sánchez N., Sestito P., de Castro E., Cornide M., Yañez Gestoso J., 2015, *ApJS*, **216**, 26
- Gomez M., Whitney B. A., Kenyon S. J., 1997, *AJ*, **114**, 1138
- Hashimoto J., Dong R., Muto T., 2021, *AJ*, **161**, 264
- Herbig G. H., Bell K. R., 1988, Third Catalog of Emission-Line Stars of the Orion Population : 3 : 1988
- Herbig G. H., Kameswara Rao N., 1972, *ApJ*, **174**, 401
- Herczeg G. J., Hillenbrand L. A., 2014, *ApJ*, **786**, 97
- Heyer M. H., Snell R. L., Goldsmith P. F., Myers P. C., 1987, *ApJ*, **321**, 370
- Himpel K., 1944, Beobachtungs-Zirkular der Astronomischen Nachrichten, **26**, 7 (3.1944)
- Howard C. D., et al., 2013, *ApJ*, **776**, 21
- Kenyon S. J., Hartmann L., 1995, *ApJS*, **101**, 117
- Kenyon S. J., Brown D. I., Tout C. A., Berlind P., 1998, *AJ*, **115**, 2491
- Kirilova T. S., Pavlovskaya E. D., 1963, *Peremennye Zvezdy*, **14**, 420
- Kulkarni A. K., Romanova M. M., 2008, *MNRAS*, **386**, 673
- Lamzin S. A., 1995, *A&A*, **295**, L20
- López-Valdivia R., et al., 2021, *ApJ*, **921**, 53
- Malyshev V. S., 1972, *Peremennye Zvezdy Prilozhenie*, **1**, 379
- Martin R. G., Lubow S. H., 2017, *ApJ*, **835**, L28
- Monin J. L., Clarke C. J., Prato L., McCabe C., 2007, in Reipurth B., Jewitt D., Keil K., eds, *Protostars and Planets V*. p. 395 ([arXiv:astro-ph/0604031](https://arxiv.org/abs/astro-ph/0604031))
- Morrissey P., et al., 2007, *ApJS*, **173**, 682
- Myers P. C., 1982, *ApJ*, **257**, 620
- Nadjip A. E., Tatarnikov A. M., Toomey D. W., Shatsky N. I., Cherepashchuk A. M., Lamzin S. A., Belinski A. A., 2017, *Astrophysical Bulletin*, **72**, 349
- Narayanan G., Snell R., Bemis A., 2012, *MNRAS*, **425**, 2641
- Nofi L. A., et al., 2021, *ApJ*, **911**, 138
- Nurmanova U. A., 1983, *Peremennye Zvezdy*, **21**, 777
- Rebull L. M., Stauffer J. R., Cody A. M., Hillenbrand L. A., Bouvier J., Roggero N., David T. J., 2020, *AJ*, **159**, 273
- Reinmuth K., 1930, *Astronomische Nachrichten*, **238**, 333
- Rodriguez J. E., et al., 2017, *ApJ*, **848**, 97
- Romanova M. M., Koldoba A. V., Ustyugova G. V., Blinova A. A., Lai D., Lovelace R. V. E., 2021, *MNRAS*, **506**, 372
- Rydgren A. E., Vrba F. J., 1983, *AJ*, **88**, 1017
- Safonov B. S., Lysenko P. A., Dodin A. V., 2017, *Astronomy Letters*, **43**, 344
- Sargent B. A., et al., 2009, *ApJ*, **690**, 1193
- Schaefer G. H., Simon M., Nelan E., Holfeltz S. T., 2003, *AJ*, **126**, 1971
- Schaefer G. H., Simon M., Beck T. L., Nelan E., Prato L., 2006, *AJ*, **132**, 2618
- Schaefer G. H., Prato L., Simon M., Patience J., 2014, *AJ*, **147**, 157
- Siess L., Dufour E., Forestini M., 2000, *A&A*, **358**, 593
- Simon M., et al., 1995, *ApJ*, **443**, 625
- Smallwood J. L., Martin R. G., Lubow S. H., 2021, *ApJ*, **907**, L14
- Tognelli E., Prada Moroni P. G., Degl'Innocenti S., 2011, *A&A*, **533**, A109
- Valenti J. A., Basri G., Johns C. M., 1993, *AJ*, **106**, 2024
- Whitney B. A., Kenyon S. J., Gómez M., 1997, *ApJ*, **485**, 703
- Whittet D. C. B., Martin P. G., Hough J. H., Rouse M. F., Bailey J. A., Axon D. J., 1992, *ApJ*, **386**, 562
- Wurster J., Bate M. R., Price D. J., 2019, *MNRAS*, **489**, 1719
- Zanazzi J. J., Lai D., 2018, *MNRAS*, **473**, 603
- Zhang Z., et al., 2018, *ApJ*, **858**, 41

This paper has been typeset from a  $\text{\TeX}/\text{\LaTeX}$  file prepared by the author.